Generating a bandwidth-tunable squeezed state via phase manipulation of entangled sideband modes

Yimiao Wu,[1] Shaoping Shi,[1,†] Xuan Liu,[1] Long Tian,[1,2] Wei Li,[1,2] Yajun Wang,[1,2] and Yaohui Zheng[1,2,*]

[1] *State Key Laboratory of Quantum Optics Technologies and Devices, Institute of Opto-Electronics, Shanxi University, Taiyuan 030006, China*

[2] *Collaborative Innovation Center of Extreme Optics, Shanxi University, Taiyuan 030006, China*

(Received 8 January 2025; revised 20 February 2025; accepted 20 March 2025; published 8 April 2025)

A squeezed state is one of the most vital quantum resources in quantum information processing. The extensive attention has increasingly shifted to not only the squeezed degree but also the squeezed bandwidth in quantum precise measurement. Here, we demonstrate the generation of a bandwidth-tunable squeezed state by exploiting the entangled sideband modes and the postprocessing scheme, with the quantum noise reduction of 8.0 ± 0.3 dB across a wide frequency range from 10 Hz to 10 MHz. Moreover, the bandwidth and rotation frequency can be conveniently manipulated in the whole frequency range according to the application requirement. There is no doubt that the demonstration will open up some potential applications about squeezed-state interaction with atoms.

DOI: 10.1103/PhysRevApplied.23.044021

I. INTRODUCTION

Squeezed light, in which the uncertainty in one of the quadratures is reduced below the shot-noise limit (SNL) and in the conjugate quadrature the uncertainty is amplified, belongs to the most common nonclassical resource [1,2]. The parametric down-conversion process has been proved to be the most successful scheme for squeezed-state generation, which has continually held the highest squeezing factor record [3–5]. Dependent on the bandwidth of optical parametric oscillator (OPO), squeezed light has an intrinsic bandwidth from several of MHz to tens of THz [6–8]. In theory, the squeezing factor is optimal at low Fourier frequency, and degrades with the increase of the Fourier frequency since the OPO is a low-pass filter [9]. Limited by the laser noise and nonlinear noise coupling, the maximum squeezing factor is at MHz with a quantum noise reduction of 15 dB, not in the audio band and even lower [4]. For the application of gravitational-wave detection, the frequency band was extended to 0.5 Hz at 1550 nm and 4 mHz at 1064 nm in virtue of the low-frequency noise-immunity technique [10,11]. On the other hand, some important applications, including atom absorption and spontaneous emission spectra measurement, need a bandwidth-tunable squeezed state with a narrow bandwidth to mitigate the line-narrowing effects of atom systems [12–14]. Unfortunately, it is unattainable to produce a squeezed state by directly manipulating the linewidth of the OPO cavity without sacrificing the squeezing factor [9]. Therefore, it is urgent that a generation scheme of a bandwidth-tunable squeezed state should be proposed to satisfy the interaction with an atomic ensemble.

In principle, we can manipulate the bandwidth of a squeezed state by rotating the squeezed angle at a predetermined frequency, confining quantum noise reduction to a small frequency range. The squeezing of a squeezed field derives from quantum correlations between each pair of symmetric sidebands around the half pump frequency [15–18]. By tuning the relative phase between the symmetric sideband modes, the correlation noise of two sideband modes changes from squeezing noise to antisqueezing noise. By the employment of an additional narrowband filter cavity (FC), the reflected sideband modes have a different phase shift that depends on the detuning from the resonant frequency, causing a rotation of squeezed angle [19–22]. The narrower the linewidth of the FC turns out to be, the lower the rotation frequency can be accurately observed. To realize the bandwidth-tunable manipulation at ultralow frequency, the FC should have ultranarrow linewidth, which faces challenges of complexity and cost [23–25]. Besides, the electromagnetically induced transparency media also can be regarded as a dispersive device to manipulate the squeezed angle by controlling the atomic density or driving field intensity [26]. The optomechanical squeezing that exploits the quantum nature of the mechanical interaction between laser and a membrane mechanical resonator also dynamically tunes the squeezed bandwidth

*Contact author: yhzheng@sxu.edu.cn
†Contact author: ssp4208@sxu.edu.cn

[27–29]. These methods mentioned above rely on additional optical components, such as external FCs, atomic vapor cells, and optomechanical coupling systems, which inevitably causes an excess loss. In a laser interferometer measurement system, utilizing the interferometer operating in a detuned configuration as both a measurement apparatus and a filter cavity, the upper and lower sidebands of the squeezed field undergo a frequency-dependent differential phase delay, resulting in a quadrature rotation. The scheme avoids an external FC that is complex and expensive. But its application is limited to the measurement system based on an interferometer [30–32].

In this paper, we present an alternative strategy for preparing a bandwidth-tunable squeezed state by utilizing the entangled sideband modes and the postprocessing technique. The squeezed state is experimentally prepared with a bandwidth from 10 Hz to 10 MHz. Subsequently, a triangular-shaped ring filter cavity (RFC) is employed as the frequency-dependent filter to separate the upper and lower sideband modes. The noise variances of the two sideband modes are measured in virtue of two pairs of balanced homodyne detectors (BHDs). We construct an algorithm that can rotate the squeezed angle with arbitrary frequency, and perform the postprocessing on the output of one of the BHDs. At last, the correlation noise between two sideband modes is obtained, demonstrating the characteristic of similar low-pass, high-pass, and band-pass filters. The demonstration provides a valuable scheme for the bandwidth-tunable squeezed state, which will open up some potential applications in atom absorption and spontaneous emission spectra measurement.

II. EXPERIMENTAL SETUP

The squeezing of a squeezed state derives from quantum correlations between each pair of symmetric sideband modes around the carrier within the phase-matching bandwidth of the nonlinear crystal [15,33]. Frequency-independent squeezed state can be directly generated from an OPO. Utilizing a local oscillator (LO) as an auxiliary beam, we can measure the correlation noise of the upper and lower sideband modes, which is equivalent to no phase delay between two sideband modes [34]. Then the squeezed angle, which is dependent on the pump phase, remains constant as shown in Fig. 1(a), generating a broadband squeezed state. Figure 1(b) shows the correlation noise of the upper and lower sideband modes at a constant (nonzero) phase delay, which presents a periodic oscillation with Fourier frequency, corresponding to a rotation of squeezed angle [6,35,36]. The oscillation period decreases with an increase in the phase delay. Therefore, we cannot independently select the bandwidth and rotation frequency. We expect to construct a like-dispersion delay model to address the problem that originates from the constant phase delay. As shown in Fig. 1(c), utilizing the postprocessing algorithm, we develop the equivalent of the FCs, converting a frequency-independent squeezed state into a frequency-dependent one. The data processing and

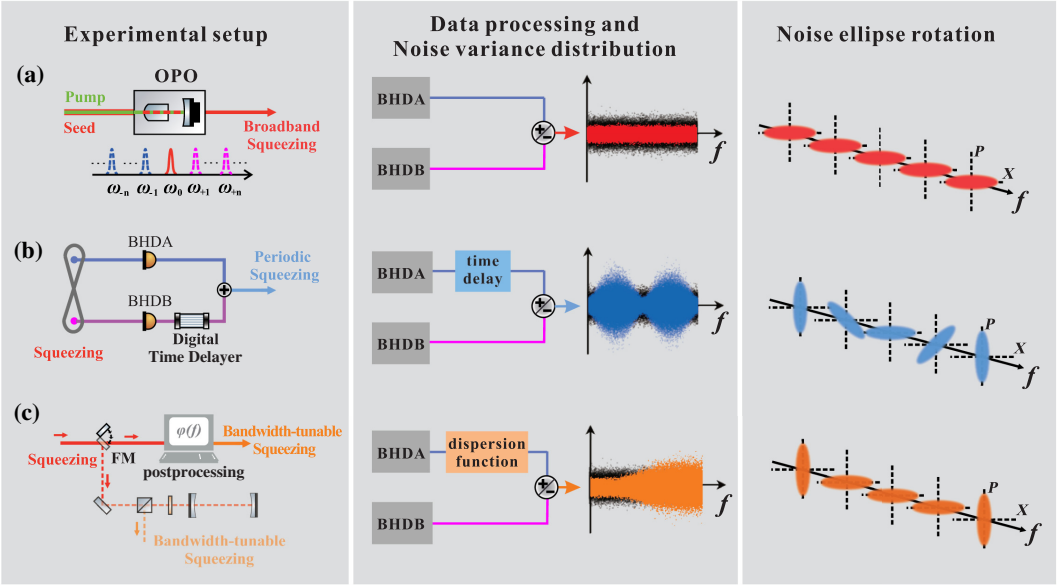

FIG. 1. Schematic of the quantum squeezed-state generation and manipulation. (a) Broadband squeezing, (b) periodic squeezing, (c) bandwidth-tunable squeezing. The first column synthesizes the experimental setup, the second column presents the data processing and noise variance distribution of the quantum squeezed states, and the third column shows the noise ellipse rotation in the sideband picture. The X and P are amplitude and phase quadrature in the phase space, respectively, and f denotes the Fourier frequency. OPO, optical parametric oscillator; BHD, balanced homodyne detector; FM, flip mirror.

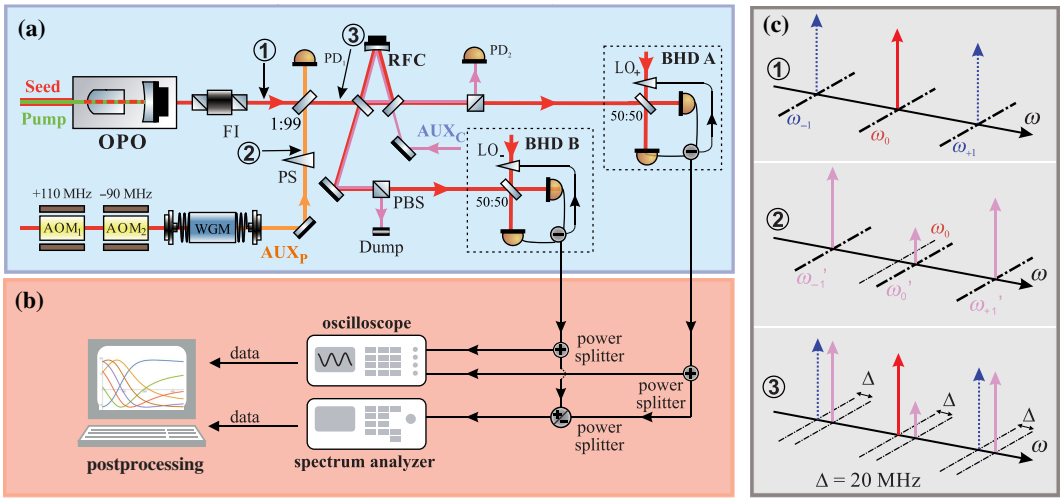

FIG. 2. Experimental setup of the bandwidth-tunable squeezed-state generation. (a) Optical unit, (b) data acquisition and analysis unit, (c) frequency diagram at three different locations in phase control loop: ① entangled sideband modes, ② phase control auxiliary beam AUX_P, ③ heterodyne beat control beam. The ω_i is the optical frequency of the carriers and sideband modes. OPO, optical parametric oscillator; FI, Faraday isolator; PS, phase shifter; RFC, ring filter cavity; AOM, acoustic-optic modulator; WGM, waveguide electro-optic phase modulator; AUX, auxiliary beam; PD, photodetector; PBS, polarization beam splitter; BHD, balanced homodyne detector; LO, local oscillator.

the noise variance distribution of the squeezed states are shown in the middle column of Fig. 1, the black curves represent the SNL. The third column shows the noise ellipse rotation in the sideband picture.

The detailed experimental setup is shown in Fig. 2. The squeezed state is produced through an OPO that is a semihemilithic optical resonator containing a periodically poled $KTiOPO_4$ (PPKTP) crystal. The design of the OPO is based on earlier experiments presented in [37–39]. The OPO has a free spectral range (FSR) of 3.325 GHz. Since high-order sideband modes have no coherent amplitude, they cannot directly obtain the error signal for the downstream experiment [36]. In the previous experiment, we employ a waveguide electro-optic phase modulator (WGM) to generate a frequency-comb-type auxiliary beam that manages the RFC and relative phase in the downstream experiment [37–39]. Unfortunately, under this scheme each vacuum sideband mode of the squeezed state has the same frequency with corresponding auxiliary control beam. Each comb of the auxiliary beam has considerably high technical noise at low frequency, which limits the generation of the low-frequency squeezed state.

To address the question, it would be specially mentioned that two additional acoustic-optic modulators (AOMs) are inserted into the optical path to generate a frequency shift of 20 MHz for each modulation sideband of the WGM. Two AOMs operate at the modulation frequencies of +110 and −90 MHz, respectively [40,41]. The WGM has a modulation frequency of 3.325 GHz, which equals the FSR of the OPO. The output from the WGM, including the carrier and modulated sidebands, acts as the phase-control auxiliary beam (AUX_P). The carrier of the AUX_P is phase locked to 0 with that of the squeezed beam via the heterodyne beat control technique. The error signal is extracted from the photodetector PD_1 with the demodulation frequency of 20 MHz [42]. For the corresponding sideband mode, the AUX_P and the squeezed state have a constant frequency difference, as shown in Fig. 2(c) [43]. Therefore, the relative phases between each sideband and its corresponding auxiliary control beam are naturally locked. The influence of weak frequency shift (20 MHz) from the entangled sideband mode on the system performance can be neglected.

The low-loss RFC, located behind the OPO, serves as a frequency-dependent beam splitter to separate the entangled sideband modes. The upper sideband mode resonates with the RFC, and thus a corresponding frequency component is transmitted, while the lower sideband mode is completely reflected. It should be noted that the RFC is primarily used to separate the sideband modes and further detect the sideband entanglement, rather than introducing the detuned phase like an optical FC for frequency-dependent squeezed-state generation. Moreover, the stable and unbiased control of the RFC length is essential for low-loss sideband separation. We employ another auxiliary beam (AUX_C) with orthogonal polarization to actively control the cavity length of the RFC. The AUX_C is reversely injected to the RFC to avoid the parasitic interference, its frequency is precisely manipulated by an AOM-based frequency-shifted unit. The separated sideband modes interfere with the corresponding LOs on a 50:50 beam splitter and are directed toward the BHDs

to measure the quantum noise. The generation of the frequency-shifting LOs is similar with our previous works [37–39]. The LO phases are simultaneously locked to 0 ($\pi/2$) by extracting the signals from the ac (dc) output of two BHDs. The signals detected by two BHDs are split into two parts via the power splitters, one is for time-domain data acquisition by an oscilloscope, another is for frequency-domain measurement via a spectrum analyzer. The time-domain data are postprocessed to generate the noise variance.

III. EXPERIMENTAL ANALYSIS AND RESULTS

With the pump power $P_1 = 175$ mW, a maximum correlation noise of 8.0 ± 0.3 dB below the SNL at the Fourier frequency from 10 Hz to 1 kHz is directly obtained from the spectrum analyzer, corresponding to an anticorrelation noise of 18.0 ± 0.4 dB. The result also serves as the reference for theoretical analysis and postprocessing result.

The noise variances of the squeezing (V_s) and antisqueezing (V_a) can be expressed as [44]:

$$V_{s/a} = 1 \mp \frac{4\eta\sqrt{P_1/P_{\text{th}}}}{\left(1 \pm \sqrt{P_1/P_{\text{th}}}\right)^2 + 4(f/\kappa)^2}, \tag{1}$$

where η is the total efficiency, P_{th} is the threshold power (280 mW), κ is the linewidth of the OPO (68 MHz), f is the Fourier frequency. The escape efficiency $\eta_{\text{esc}} = T/(T+L)$ of the OPO is 98.3%, dependent of the coupling mirror power transmissivity T and the intracavity round-trip loss L. The propagation efficiency η_{prop} is 95.0%, the electronic efficiency η_{ele} is 99.7%, the quantum efficiency η_{photo} of the photodiode is 99.0%, and the homodyne contrast efficiency η_{vis} is 97.0%. From these results, we estimated the system total efficiency as [4]

$$\eta = \eta_{\text{esc}}\eta_{\text{prop}}\eta_{\text{ele}}\eta_{\text{photo}}\eta_{\text{vis}} > 89.0\%. \tag{2}$$

Except for the optical loss, the phase fluctuation between the signal and LO field changes the noise variances distribution in phase and amplitude quadrature. When the phase fluctuation θ is considered, the noise variance accordingly changes as

$$V_s' = V_s \cos^2\theta + V_a \sin^2\theta. \tag{3}$$

In our prior work about the generation of broadband-entangled sideband modes [6], the constant time delay caused by the resonance RFC has been analyzed, which leads to the degradation of the quantum correlation noise in the high-frequency band. Via an electronic delay compensation scheme, the broadband frequency-independent entangled sideband modes are experimentally obtained. The same phenomenon is also verified in four-wave mixing system, where different group velocities between the correlated probe and conjugate signals leads to the similar results [35,45]. Consequently, the noise variance exhibits periodic oscillations with the Fourier frequency f and the time delay t. In this context, the noise variance can be described as follows:

$$V_{\text{periodic}} = V_s \cos^2(tf\pi + \theta) + V_a \sin^2(tf\pi + \theta). \tag{4}$$

Figure 3 presents the measurement results and theoretical curves of the correlation noise at a constant phase delay, with the noise power normalized to the SNL. To construct an apparent oscillation in the squeezing spectrum at low frequency, a long-time delay between the upper and lower sideband modes is required. However, realizing lossless time delay presents significant challenges in the actual experiment. In order to overcome the limitation, we adopt a postprocessing technique, which involves manipulating the time-domain signal. The time-domain data of the BHD A and BHD B are acquired through the oscilloscope (MDO3014, Tektronix), which has a sampling rate f_s of 2 kS/s, a sampling time of 1 s, corresponding to the total samples N of 2000. There exists a time interval of 0.5 ms between each sample. From these parameters, we can infer that the frequency range of the collected data is from 1 Hz ($f_{\text{min}} = f_s/N$) to 1 kHz ($f_{\text{max}} = f_s/2$). As shown in Fig. 3 (10 Hz–1 kHz), the blue horizontal line represents the SNL that is collected by blocking the squeezed beam. By artificially introducing time delays (1, 2, and 3 ms) and adding the two sets of data from BHD A and BHD B, we can further process these data using the LPSD (logarithmic frequency axis power spectral density) algorithm and obtain the relative noise power spectrum [46]. The correlated noises with different periods are represented by the yellow, green, and purple traces in Fig. 3, respectively. The squeezed angle exhibits periodic rotation instead of remaining fixed at a single transition frequency point. It should be emphasized that these measurements were conducted when both LOs phases were locked at 0. The spikes detected at frequencies such as 25 and 50 Hz can be ascribed to the electrical crosstalk from the power supply module.

To generate the bandwidth-tunable squeezed state, a dispersion function model is employed to complete the noise ellipse rotation. Introduced the differential phase in one half of symmetric sideband modes, the relative phase as a function of the Fourier frequency, could be expressed as [47,48]

$$\varphi_s(f) = \pi + \frac{1}{2}\arg[\rho(f)], \tag{5}$$

$$\rho(f) = \frac{\sqrt{R_1} - \sqrt{R_2}e^{i2\pi(f-f_d)/\delta}}{1 - \sqrt{R_1R_2}e^{i2\pi(f-f_d)/\delta}}, \tag{6}$$

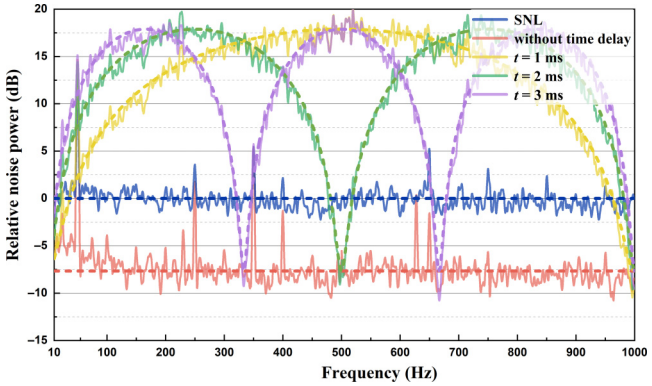

FIG. 3. Relative noise power spectrum of the periodic squeezing, which is generated by introducing a constant phase delay. The digital time delays of 1, 2, and 3 ms correspond to the yellow, green, and purple lines, respectively. The experimental data (solid lines) are in good agreement with analysis results (dashed lines).

where the $\rho(f)$ is the transfer function, R_1 and R_2 are the power reflectivities of the input and output coupling mirror, δ is the FSR of the optical resonator, and f_d is the cavity detuning frequency. The noise variance of the bandwidth-tunable squeezed state is

$$V_{\text{bandwidth tunable}} = V_s \cos^2[\varphi - \varphi_s(f)] + V_a \sin^2[\varphi - \varphi_s(f)], \quad (7)$$

where φ is the readout angle, which determines the direction of the squeezed ellipse projected. The generation mechanism of the bandwidth-tunable squeezed state can be understood through a sideband picture, where the squeezed angle is determined by the relative phase between the upper and lower sidebands at each frequency. The upper sideband is at far detuning, while the lower sideband reflected from the optical resonator has a frequency-dependent phase delay, resulting in the squeezed angle rotation.

Figure 4 shows the relative noise power spectrum of the bandwidth-tunable squeezed state by the employment of the postprocessing method. The time-domain signals from BHD A and BHD B are simultaneously collected in a similar manner, then sent to postprocessing. With the time delay of 0, by performing the addition (subtraction) algorithm for the two sets of data, we can obtain the correlated noise spectrum V_s (anticorrelated noise spectrum V_a), as shown in Fig. 4(a). The black curves are SNL, which are obtained by only injecting LO field into the BHDs, and the red curves and blue curves are the squeezing and antisqueezing noise spectrum, respectively. The correlated noise variance has a quantum noise reduction of 8.0 ± 0.3 dB at the Fourier frequency of 10 Hz–10 MHz, while the anticorrelated noise variance is amplified to 18.0 ± 0.4 dB. The processing results of time-domain

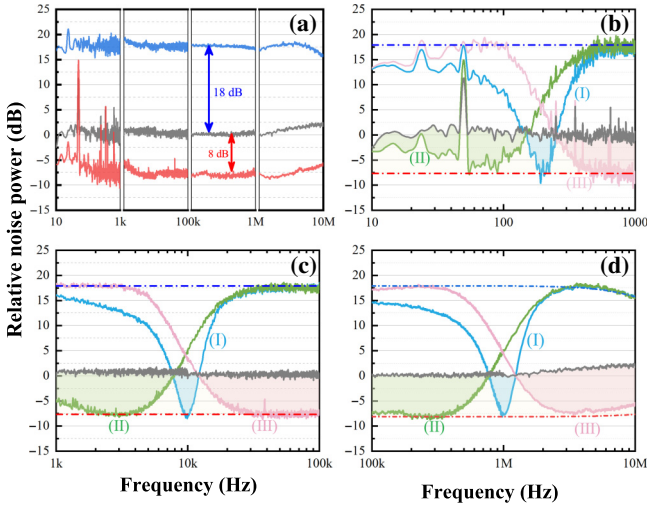

FIG. 4. Relative noise power spectra of the bandwidth-tunable squeezing. (a) Measured relative noise power spectra of the broadband squeezing from 10 Hz–10 MHz. The black, red, and blue curves represent the shot-noise limit, squeezing, and antisqueezing noise, respectively. (b)–(d) Relative noise power spectra of the bandwidth-tunable squeezing with different squeezed frequency range. Trace (I)–(III) represent the band-pass, low-pass, and high-pass filters, respectively.

data are in good agreement with the measurement result ones that utilizes the spectrum analyzer. Subsequently, we perform the time delay for one of the time-domain signals by employing a dispersion function model analyzed above. The processing results are added (subtracted) with another time-domain signal, obtaining the relative noise power spectrum of bandwidth-tunable squeezing shown in Figs. 4(b)–4(d). In the three illustrations, curve (I) represents the band-pass result, which are prepared under the condition that the optical resonator is at semidetuning and the detection phase is locked to $\pi/2$. In a similar way, we can generate the squeezed state with a quantum noise reduction at low frequency [curve (II)] or at high frequency [curve (III)], which corresponds to the low-pass and high-pass filters. All these results are normalized to the vacuum noise. During this process, multiple parameters, including the detuning amount, the linewidth of the optical resonator, and the readout angle, are optimized for different frequency bands. The demonstration provides a valuable generation scheme of the bandwidth-tunable squeezed state.

IV. CONCLUSION

In summary, we have generated a bandwidth-tunable squeezed state in virtue of the postprocessing technique. Thanks to the generation of the low-frequency squeezed state in our previous work [11], the bandwidth-tunable squeezed state has a quantum noise reduction of 8.0 ± 0.3 dB across a wide frequency range from 10 Hz to

10 MHz. We have constructed an algorithm that simulates the squeezed angle rotation with arbitrary frequency, demonstrating the noise characteristic of similar low-pass, high-pass, and band-pass filters. Furthermore, the rotation frequency can be conveniently manipulated according to the application requirement. The flexible scheme will open up some potential applications about squeezed-state interaction with atoms.

ACKNOWLEDGMENTS

This work is supported by the National Natural Science Foundation of China (Grants No. 62225504, No. 62027821, No. U22A6003, No. 62035015, No. 12174234, and No. 12304399); Fundamental Research Program of Shanxi Province (Grants No. 202303021212003, and No. 202303021224006).

DATA AVAILABILITY

The data that support the findings of this study are available from the corresponding authors upon reasonable request.

[1] D. F. Walls, Squeezed states of light, Nature **306**, 141 (1983).
[2] R. E. Slusher, L. W. Hollberg, B. Yurke, J. C. Mertz, and J. F. Valley, Observation of squeezed states generated by four-wave mixing in an optical cavity, Phys. Rev. Lett. **55**, 2409 (1985).
[3] L. Wu, H. J. Kimble, J. L. Hall, and H. Wu, Generation of squeezed states by parametric down conversion, Phys. Rev. Lett. **57**, 2520 (1986).
[4] H. Vahlbruch, M. Mehmet, K. Danzmann, and R. Schnabel, Detection of 15 dB squeezed states of light and their application for the absolute calibration of photoelectric quantum efficiency, Phys. Rev. Lett. **117**, 110801 (2016).
[5] T. Serikawa, J. Yoshikawa, K. Makino, and A. Frusawa, Creation and measurement of broadband squeezed vacuum from a ring optical parametric oscillator, Opt. Express **24**, 28383 (2016).
[6] S. Shi, Y. Wu, L. Gao, L. Zheng, L. Tian, Y. Wang, W. Li, and Y. Zheng, Generating six pairs of bandwidth-expanded entangled sideband modes via time delay compensation, Opt. Lett. **48**, 3111 (2023).
[7] R. Nehra, R. Sekine, L. Ledezma, Q. Guo, R. M. Gray, A. Roy, and A. Marandi, Few-cycle vacuum squeezing in nanophotonics, Science **377**, 1333 (2022).
[8] T. Kashiwazaki, N. Takanashi, T. Yamashima, T. Kazama, K. Enbutsu, R. Kasahara, T. Umeki, and A. Furusawa, Continuous-wave 6-dB-squeezed light with 2.5-THz-bandwidth from single-mode PPLN waveguide, APL Photonics **5**, 036104 (2020).
[9] R. Schnabel, Squeezed states of light and their applications in laser interferometers, Phys. Rep. **684**, 1 (2017).
[10] F. Meylahn, B. Willke, and H. Vahlbruch, Squeezed states of light for future gravitational wave detectors at a wavelength of 1550 nm, Phys. Rev. Lett. **129**, 121103 (2022).
[11] L. Gao, L. Zheng, B. Lu, S. Shi, L. Tian, and Y. Zheng, Generation of squeezed vacuum state in the millihertz frequency band, Light: Sci. Appl. **13**, 294 (2024).
[12] M. Bosticky, Z. Ficek, and B. J. Dalton, Probe absorption spectra for driven atomic systems in a narrow bandwidth squeezed vacuum, Phys. Rev. A **53**, 4439 (1996).
[13] M. R. Ferguson, Z. Ficek, and B. J. Dalton, Phase-dependent fluorescence linewidth narrowing in a three-level atom damped by a finite-bandwidth squeezed vacuum, Phys. Rev. A **56**, 4125 (1997).
[14] E. S. Polzik, J. Carri, and H. J. Kimble, Atomic spectroscopy with squeezed light for sensitivity beyond the vacuum-state limit, Appl. Phys. B **55**, 279 (1992).
[15] B. Hage, A. Samblowski, and R. Schnabel, Towards Einstein-Podolsky-Rosen quantum channel multiplexing, Phys. Rev. A **81**, 062301 (2010).
[16] E. H. Huntington and T. C. Ralph, Separating the quantum sidebands of an optical field, J. Opt. B: Quantum Semiclassical Opt. **4**, 123 (2002).
[17] G. Breitenbach, S. Schiller, and J. Mlynek, Measurement of the quantum states of squeezed, Nature **387**, 471 (1997).
[18] D. Wilken, J. Junker, and M. Heurs, Broadband detection of 18 teeth in an 11-dB squeezing comb, Phys. Rev. Appl. **21**, L031002 (2024).
[19] W. Jia, V. Xu, K. Kuns, M. Nakano, L. Barsotti, M. Evans, and N. Mavalvala, Members of the LIGO Scientific Collaboration, Squeezing the quantum noise of a gravitational-wave detector below the standard quantum limit, Science **385**, 1318 (2024).
[20] D. Ganapathy, *et al.*, LIGO O4 Detector Collaboration, Broadband quantum enhancement of the LIGO detectors with frequency-dependent squeezing, Phys. Rev. X **13**, 041021 (2023).
[21] L. McCuller, C. Whittle, D. Ganapathy, K. Komori, M. Tse, A. Fernandez-Galiana, L. Barsotti, P. Fritschel, M. MacInnis, F. Matichard, K. Mason, N. Mavalvala, R. Mittleman, H. Yu, M. E. Zucker, and M. Evans, Frequency-dependent squeezing for advanced LIGO, Phys. Rev. Lett. **124**, 171102 (2020).
[22] Y. Zhao, *et al.*, Frequency-dependent squeezed vacuum source for broadband quantum noise reduction in advanced gravitational-wave detectors, Phys. Rev. Lett. **124**, 171101 (2020).
[23] M. Evans, L. Barsotti, P. Kwee, J. Harms, and H. Miao, Realistic filter cavities for advanced gravitational wave detectors, Phys. Rev. D **88**, 022002 (2013).
[24] E. Capocasa, M. Barsuglia, J. Degallaix, L. Pinard, N. Straniero, R. Schnabel, K. Somiya, Y. Aso, D. Tatsumi, and R. Flaminio, Estimation of losses in a 300 m filter cavity and quantum noise reduction in the KAGRA gravitational-wave detector, Phys. Rev. D **93**, 082004 (2016).
[25] E. Capocasa, Y. Guo, M. Eisenmann, Y. Zhao, A. Tomura, K. Arai, Y. Aso, M. Marchiò, L. Pinard, P. Prat, K. Somiya, R. Schnabel, M. Tacca, R. Takahashi, D. Tatsumi, M. Leonardi, M. Barsuglia, and R. Flaminio, Measurement of optical losses in a high-finesse 300 m filter cavity for broadband quantum noise reduction in gravitational-wave detectors, Phys. Rev. D **98**, 022010 (2018).

[26] E. E. Mikhailov, K. Goda, T. Corbitt, and N. Mavalvala, Frequency-dependent squeeze-amplitude attenuation and squeeze-angle rotation by electromagnetically induced transparency for gravitational-wave interferometers, Phys. Rev. A **73**, 053810 (2006).

[27] Y. Ma, S. L. Danilishin, C. Zhao, H. Miao, W. Z. Korth, Y. Chen, R. L. Ward, and D. G. Blair, Narrowing the filter-cavity bandwidth in gravitational-wave detectors via optomechanical interaction, Phys. Rev. Lett. **113**, 151102 (2014).

[28] T. P. Purdy, P.-L. Yu, R. W. Peterson, N. S. Kampel, and C. A. Regal, Strong optomechanical squeezing of light, Phys. Rev. X **3**, 031012 (2013).

[29] B. Xiong, X. Li, S. Chao, Z. Yang, W. Zhang, W. Zhang, and L. Zhou, Strong mechanical squeezing in an optomechanical system based on Lyapunov control, Photonics Res. **8**, 151 (2020).

[30] Y. Ma, H. Miao, B. H. Pang, M. Evans, C. Zhao, J. Harms, R. Schnabel, and Y. Chen, Proposal for gravitational-wave detection beyond the standard quantum limit through EPR entanglement, Nat. Phys. **13**, 776 (2017).

[31] J. Südbeck, S. Steinlechner, M. Korobko, and R. Schnabel, Demonstration of interferometer enhancement through Einstein–Podolsky–Rosen entanglement, Nat. Photonics **14**, 240 (2020).

[32] M. J. Yap, P. Altin, T. G. McRae, B. J. J. Slagmolen, R. L. Ward, and D. E. McClelland, Generation and control of frequency-dependent squeezing via Einstein–Podolsky–Rosen entanglement, Nat. Photonics **14**, 223 (2020).

[33] J. Zhang, Einstein-Podolsky-Rosen sideband entanglement in broadband squeezed light, Phys. Rev. A **67**, 054302 (2003).

[34] W. Li, Y. Jin, X. Yu, and J. Zhang, Enhanced detection of a low-frequency signal by using broad squeezed light and a bichromatic local oscillator, Phys. Rev. A **96**, 023808 (2017).

[35] L. E. E. de Araujo, Z. Zhou, M. DiMario, B. E. Anderson, J. Zhao, K. M. Jones, and P. D. Lett, Characterizing two-mode-squeezed light from four-wave mixing in rubidium vapor for quantum sensing and information processing, Opt. Express **32**, 1305 (2024).

[36] E. H. Huntington, G. N. Milford, C. Robilliard, T. C. Ralph, O. Glöckl, U. L. Andersen, S. Lorenz, and G. Leuchs, Demonstration of the spatial separation of the entangled quantum sidebands of an optical field, Phys. Rev. A **71**, 041802 (2005).

[37] S. Shi, L. Tian, Y. Wang, Y. Zheng, C. Xie, and K. Peng, Demonstration of channel multiplexing quantum communication exploiting entangled sideband modes, Phys. Rev. Lett. **125**, 070502 (2020).

[38] Y. Wu, Q. Wang, L. Tian, X. Zhang, J. Wang, S. Shi, Y. Wang, and Y. Zheng, Multi-channel multiplexing quantum teleportation based on the entangled sideband modes, Photonics Res. **10**, 1909 (2022).

[39] S. Shi, Y. Wang, L. Tian, W. Li, Y. Wu, Q. Wang, Y. Zheng, and K. Peng, Continuous variable quantum teleportation network, Laser Photonics Rev. **17**, 2200508 (2023).

[40] S. Chelkowski, H. Vahlbruch, K. Danzmann, and R. Schnabel, Coherent control of broadband vacuum squeezing, Phys. Rev. A **75**, 043814 (2007).

[41] D. Ganapathy, V. Xu, W. Jia, C. Whittle, M. Tse, L. Barsotti, M. Evans, and L. McCuller, Probing squeezing for gravitational-wave detectors with an audio-band field, Phys. Rev. D **105**, 122005 (2022).

[42] G. J. Verbiest and M. J. Rost, Beating beats mixing in heterodyne detection schemes, Nat. Commun. **6**, 6444 (2015).

[43] D. W. Gould, V. B. Adya, S. S. Y. Chua, J. Junker, D. Wilken, T. G. McRae, B. J. J. Slagmolen, M. J. Yap, R. L. Ward, M. Heurs, and D. E. McClelland, Quantum enhanced balanced heterodyne readout for differential interferometry, Phys. Rev. Lett. **133**, 063602 (2024).

[44] P. K. Lam, T. C. Ralph, B. C. Buchler, D. E. McClelland, H.-A. Bachor, and J. Gao, Optimization and transfer of vacuum squeezing from an optical parametric oscillator, J. Opt. B: Quantum Semiclassical Opt. **1**, 469 (1999).

[45] A. M. Marino, R. C. Pooser, V. Boyer, and P. D. Lett, Tunable delay of Einstein-Podolsky-Rosen entanglement, Nature **457**, 859 (2009).

[46] M. Tröbs and G. Heinzel, Improved spectrum estimation from digitized time series on a logarithmic frequency axis, Measurement **39**, 120 (2006).

[47] S. Chelkowski, H. Vahlbruch, B. Hage, A. Franzen, N. Lastzka, K. Danzmann, and R. Schnabel, Experimental characterization of frequency-dependent squeezed light, Phys. Rev. A **71**, 013806 (2005).

[48] E. Oelker, T. Isogai, J. Miller, M. Tse, L. Barsotti, N. Mavalvala, and M. Evans, Audio-band frequency-dependent squeezing for gravitational-wave detectors, Phys. Rev. Lett. **116**, 041102 (2016).